Molecular Therapy
Nucleic Acids
Original Article

Gene dosage effects of poly(A) track-engineered hypomorphs

Geralle Powell,[1] Slavica Pavlovic Djuranovic,[1] and Sergej Djuranovic[1]

[1]Department of Cell Biology and Physiology, Washington University School of Medicine, 600 South Euclid Avenue, Campus Box 8228, St. Louis, MO 63110, USA

Manipulation of gene activity through creation of hypomorphic mutants has been a long-standing tool in examining gene function. Our previous studies have indicated that hypomorphic mutants could be created by inserting *cis*-regulatory sequences composed of consecutive adenosine nucleotides called poly(A) tracks. Here we use poly(A) tracks to create hypomorphic mutants and functional characterization of membrane, secretory, and endogenous proteins. Insertion of poly(A) tracks into the sequences of interleukin-2 and membrane protein CD20 results in a programmable reduction of mRNA stability and attenuation of protein expression regardless of the presence of a signaling sequence. Likewise, CRISPR-Cas9 targeted insertion of poly(A) tracks into the coding sequence of the endogenous human genes *AUF1* and *TP53* results in a programmable reduction of targeted protein and mRNA levels. Functional analyses of AUF1-engineered hypomorphs indicate a direct correlation between *AUF1* gene levels and the stability of AUF1-regulated mRNAs. Hypomorphs of TP53 affect expression of the target genes differentially depending on the severity of the hypomorphic mutation. Finally, decreases in TP53 protein affect the same cellular pathways in poly(A) track-engineered cells as in cancer cells, indicating these variants' biological relevance. These results highlight this technology's power to create predictable, stable hypomorphs in recombinant or endogenous genes in combination with CRISPR-Cas9 engineering tools.

INTRODUCTION

Investigation of a gene's phenotype and its functional importance has often occurred by creating loss-of-function (LOF) mutations. LOF mutations allow examination of phenotype when gene expression is reduced (as with hypomorphic mutations) or completely ablated (as with "null" mutations).[1] However, phenotypic investigation of LOF mutations can be troublesome because of embryonic lethality or disruption of organismal development as a result of pleiotropy.[2,3] Therefore, use of hypomorphic mutations is often preferable and more experimentally advantageous.

There are several methods for creating hypomorphic mutations. Historically, chemical and UV irradiation mutagenesis screens followed by selection for phenotypic strength have been used to identify hypomorphic alleles.[1,4-6] Hypomorphic mutations have also been created through non-directed insertional mutagenesis using transposable elements in or near regulatory regions.[7,8] RNAi has also been an essential tool in creating hypomorphic phenotypes because of varying degrees of residual gene expression produced from knockdown.[9-11] However, each method of creation of hypomorphic mutations is accompanied by disadvantages. Although advances in next-generation sequencing have reduced the time and tediousness associated with finding phenotypic variants in traditional forward genetics screens, the process still requires creating a mapping population, with mapping resolution being variable.[12-14] Even when an allele is mapped to a gene of interest, mutagenesis screens still produce many other types of alleles, such as neomorphs (altered or unique function), nulls (LOF), and hypermorphs (gain of function). On the other hand, RNAi results in variable gene knockdown and can have off-target effects.[15] Therefore, there is a need for a method that can be used for all recombinant coding genes and, in combination with novel CRISPR-Cas9 technologies, to engineer endogenous genes.

We have previously described poly(A) tracks as stretches of adenosine nucleotides that decrease mRNA stability during the elongation phase of mRNA translation, causing ribosomal stalling and frameshifting.[16] The direct consequence of these events is a decrease in protein expression and mRNA stability.[16-20] The decrease in the amount of gene expression directly correlates with the length of the poly(A) track: the longer the poly(A) track, the lower the mRNA's stability and expression of the protein products.[16,17,19,20] Our previous work indicated that poly(A) tracks could be used to create hypomorphic levels of recombinant cytoplasmic proteins in various reporters and across multiple organisms, such as *E.coli*, *S. cerevisiae*, *T. thermophile*, and *N. benthamiana* and in *Drosophila* and human cells.[19] Additional studies have indicated that the same technology can be used in *C. albicans* and *A. thaliana* cells, where constructs with poly(A) tracks were inserted into previously engineered knockout cells.[20]

Previous studies of poly(A) track hypomorphs have been limited to reporters or recombinant cytoplasmic proteins and were not tested in secretory or membrane proteins.[19] Because the sequence and structure of the N terminus of secretory and transmembrane proteins are

Received 17 February 2021; accepted 1 October 2021;
https://doi.org/10.1016/j.omtn.2021.10.005.

Correspondence: Sergej Djuranovic, Department of Cell Biology and Physiology, Washington University School of Medicine, 600 South Euclid Avenue, Campus Box 8228, St. Louis, MO 63110, USA.
E-mail: sergej.djuranovic@wustl.edu

essential for co-translational translocation and, thus, proper processing and transport, it remains unclear whether insertion of poly(A) tracks would create hypomorphic mutants of such genes.[21-23] Moreover, it is still unknown whether poly(A) tracks could be engineered in endogenous genes by using the CRISPR-Cas9 system.

In this work, we show how insertion of poly(A) tracks into genes for integral membrane-spanning 4A1 (referred to hereafter as CD20) and secretory IL-2 (interleukin-2) regulates their recombinant protein expression. Inserting a poly(A) track of at least 9 and up to 18 adenosines reduces mRNA stability and protein synthesis in a programmable way without affecting protein membrane insertion or secretion out of the cells. This effect is also independent of the presence of the signaling peptide sequence in IL-2, where insertion of a poly(A) track immediately before and after the signal sequence results in a similar protein and mRNA reduction. We show that the same effects can be observed when poly(A) track sequences are introduced into endogenous genes in human tissue cultures using CRISPR-Cas9 technology. AUF1(AU-rich element RNA-binding protein 1) and TP53 (tumor protein p53) mRNA stability and protein expression are reduced in a programmable way, depending on the length of poly(A) tracks. Analyses of downstream effects of AUF1 hypomorphs indicate changes in the abundance of MAT1A (methionine adenosyltransferase 1A), APP (β-amyloid precursor protein), TOP2A (DNA topoisomerase II alpha), and USP1 (ubiquitin-specific peptidase 1) mRNAs, shown previously to respond to AUF1 protein.[24,25] Inserting poly(A) tracks in the TP53 locus of HAP1 cells leads to partial or near-complete loss of TP53 protein and TP53 dosage-dependent effects on multiple TP53-regulated genes. Our data also indicate that partial or more complete loss of *TP53* gene expression leads to downregulation of *MGMT* (O-6-methylguanine-DNA methyltransferase) gene products, a trend observed in engineered cells and cancer cell lines with compromised levels of TP53 protein.

Overall, the poly(A) track method successfully creates hypomorphic mutations in secretory and membrane proteins as well as in endogenous genes. We also show successful application of this method in haploid and diploid genomes. Finally, creation of hypomorphic mutants using CRISPR-Cas9 in conjunction with poly(A) track sequence insertion allows controlled investigation of downstream genes and pathways. This method provides titratable gene expression in a feasible and experimentally tractable way.

RESULTS

Insertion of poly(A) tracks creates hypomorphic mutants of the membrane gene CD20

To investigate whether poly(A) track technology can be used for membrane proteins, we focused on CD20.[26] CD20 is a B lymphocyte-specific integral membrane protein essential for differentiation of these cells.[27] As a member of the membrane-spanning 4A gene family encoded by the MS4A1 gene, CD20 is a 33- to 37-kDa protein with four hydrophobic transmembrane helices, one intracellular loop, and two extracellular loops with cytosolic N and C termini, respectively.[28] Because CD20 lacks an N-terminal signal peptide, its correct expression and translocation depend on its first transmembrane domain.[27-29]

To test whether insertion of poly(A) tracks can lead to programmable expression of CD20, we cloned the full sequence of CD20 into the pDEST40 vector and inserted poly(A) tracks of 12 adenosines (12As, sequence equivalent to 4 consecutive lysine AAA codons) and 18As (sequence equivalent to 6 lysine AAA codons), respectively, after the second amino acid (Figure 1A). We transfected wild-type (WT) and mutated CD20 reporters together with a Green Fluorescence Protein - Yellow Fluorescence Protein (GFP-YFP) reporter as a normalization control into Chinese hamster ovary (CHO) cells. Using qRT-PCR and western blot analysis, we examined the effects of poly(A) insertion on CD20 mRNA stability and protein expression (Figures 1B and 1C). The recombinant CD20 protein was visualized using a polyclonal CD20 antibody and compared with expression of GFP-YFP constructs. Expression of the CD20 protein was decreased over approximately 50% and 80% for reporters with insertion of 12As and 18As, respectively (Figure 1B), with previously observed degradation bands at 25 kDa.[29] We observed similar, approximately 50% and 70% reductions in mRNA stability for constructs with insertion of 12As and 18As, respectively (Figure 1C).

To investigate whether insertion of poly(A) tracks and expression of CD20 protein with short poly-lysine repeats interferes with cellular localization of this membrane-integral protein, we used live-cell imaging (Figure 2A) and flow cytometry analysis (Figure 2B). Using a fluorescein isothiocyanate (FITC)-labeled CD20-2H7-specific antibody, we performed live-cell imaging of CHO cells expressing WT CD20 and poly(A) track variants. The monoclonal CD20 antibody 2H7 binds an epitope found in the larger extracellular loop of CD20 and has been used for depletion of B cells.[30,31] Antibody immunofluorescence indicated that all three variants of CD20 are expressed in the membrane of CHO cells.[32] Furthermore, the position of the FITC-labeled CD20-2H7-specific antibody indicated a distribution of CD20 similar to the CellMask Orange plasma membrane stain (Figure 2A; Figure S1). The difference in the levels of cellular immunofluorescence was similar to the difference in protein levels seen in western blot analyses (Figure 1B). Cells expressing the WT CD20 construct had the highest immunofluorescence signal, whereas poly(A) track-engineered constructs had a programmable reduction in the abundance of the CD20 protein. CD20 protein with insertion of a poly(A) track of 12As had higher immunofluorescence than CD20 with 18As. Flow cytometry of transfected CHO cells with a FITC-labeled CD20-antibody also indicated detectable levels of expression of WT CD20 and CD20 with a poly(A) track of 12As (Figure 2B).[33]

Insertion of a poly(A) tracks creates hypomorphic mutants of secretory IL-2 protein regardless of signaling peptide

To test the ability to create hypomorphic mutants using poly(A) tracks in secretory proteins, we created reporter genes with the full-length sequence of IL-2. IL-2 is a cytokine necessary for homeostasis of T lymphocytes and clonal expansion of regulatory T cells.[34,35] As a secretory protein, IL-2 contains an N-terminal signal peptide for recognition by the signal recognition particle and efficient co-translational translocation. It has been shown previously that modification

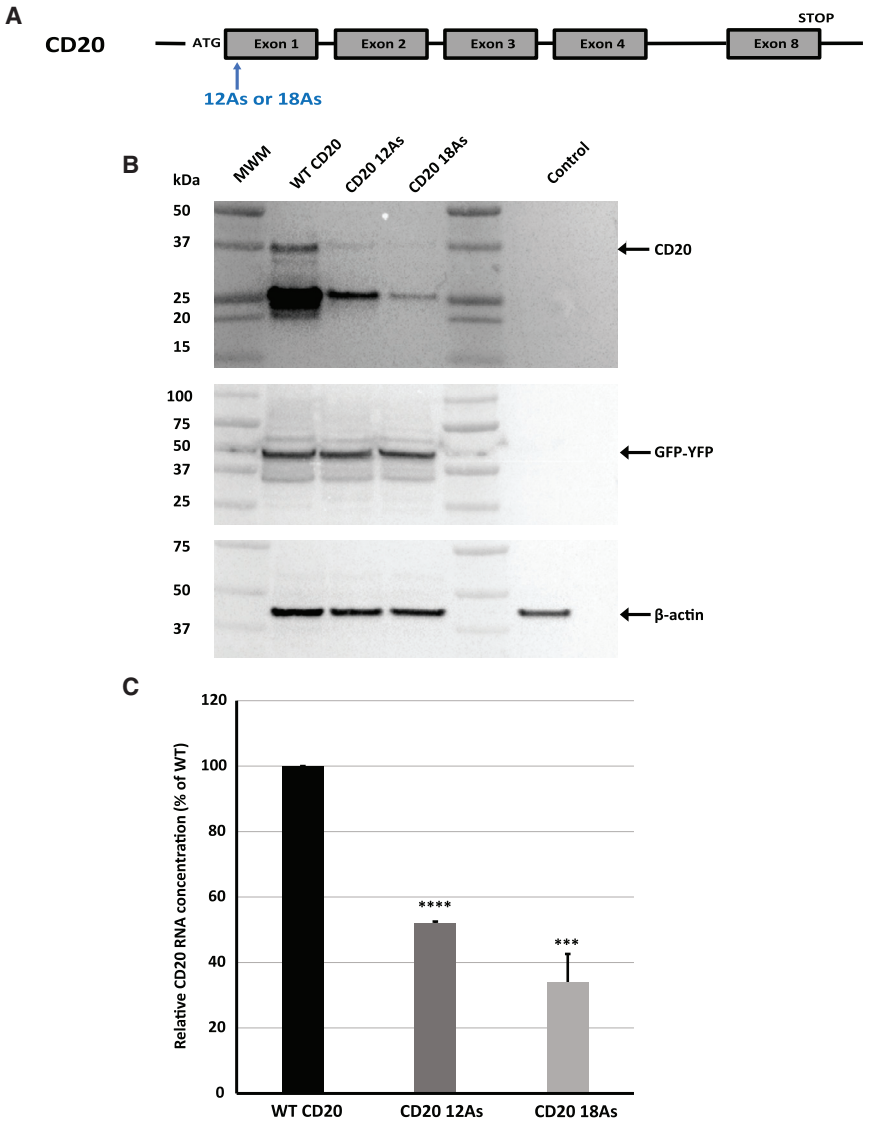

Figure 1. Design and effect of poly(A) track insertion on CD20 stability and expression

(A) Scheme representative of poly(A) insertions and location of insertions for CD20 reporter constructs used in this study. Poly(A) insertions in the CD20 coding sequence were placed proximal to the ATG start codon. A schematic of the *CD20* gene with the start codon (ATG), termination codon (STOP), and exons and insertion sites is also shown. (B) Western blot analysis of CD20 constructs expressed transiently in CHO cells. An equal amount of total protein was used for analysis. GFP-YFP and β-actin were used as transfection and loading controls, respectively, with expression of both proteins detected using specific antibodies. CD20 was detected with a CD20-specfic antibody. Arrows indicate the position of full-length CD20, GFP-YFP, and β-actin proteins. (C) mRNA levels of CD20 constructs were measured by qRT-PCR. CD20 expression was normalized to β-actin. Relative mRNA levels for both constructs (12As and 18As) are presented as percentages of WT CD20. Error bars represent mean ± SD (n = 3). p values represent significance (*$p \leq 0.05$, **$p \leq 0.01$, ***$p \leq 0.001$, ****$p \leq 0.0001$).

of the signal peptide of IL-2 could affect IL-2 expression and secretion.[36]

To test the locational flexibility of poly(A) insertion, we placed poly(A) tracks of 9As, 12As, and 18As, respectively, before and after the signal peptide sequence (Figure 3A). Poly(A) tracks before the signal peptide were inserted after the codon for the second amino acid, whereas insertion after the signal peptide sequence occurred following the codon for amino acid 27. We transfected WT IL-2 and IL-2 reporters with poly(A) track insertions into human embryonic kidney 293 (HEK293) cells. These cells have been shown previously to produce secreted IL-2 protein when transfected with recombinant IL-2.[37,38] We assayed mRNA amounts by qRT-PCR analysis for all reporters. RNA levels were reduced by approximately 20%, 40%, and 50% for 9As, 12As, and 18As, respectively, for poly(A) tracks inserted before the signal sequence and 30%, 50%, and 70% for poly(A) tracks inserted after the signal sequence, respectively (Figure 3B). We used cell medium to measure the amount of secreted IL-2 protein 48 h after transfection and applied it to a standardized IL-2 sandwich ELISA (Thermo Fisher Scientific, EH2IL2). To check the linearity of the IL-2 ELISA, we diluted WT IL-2 samples from 2- and up to 16-fold and used medium from untransfected cells as a control (WT NI - wild type no insert construct). Similar to the mRNA experiments, protein expression was reduced in IL-2 variants with poly(A) tracks regardless of position respective to the signal peptide sequence (Figure 3C). Insertion of 9As, 12As, or 18As consistently led to 60%–70%, 80%, or more than 90% reduction in IL-2 levels, as detected by ELISA (Figure 3C), regardless of whether insertion of the poly(A) track was before or after the signal peptide.

Finally, to test the functionality of the IL-2 variants with poly(A) tracks, we used an IL-2 cell-based assay (IL2 Bioassay, Promega), which reports stimulation of the IL-2 receptor through expression of the luciferase reporter (Figure 3D). Results for supernatants of the WT IL-2 sample or IL-2 variants with poly(A) tracks indicated functionally active proteins, regardless of the position of poly(A) track to encoded signaling peptide. Moreover, the luminescence levels from the functional IL-2 assay indicated a change in the levels of IL-2 protein and poly(A) track hypomorphs similar to what we observed previously in ELISA assays (Figure 3B).

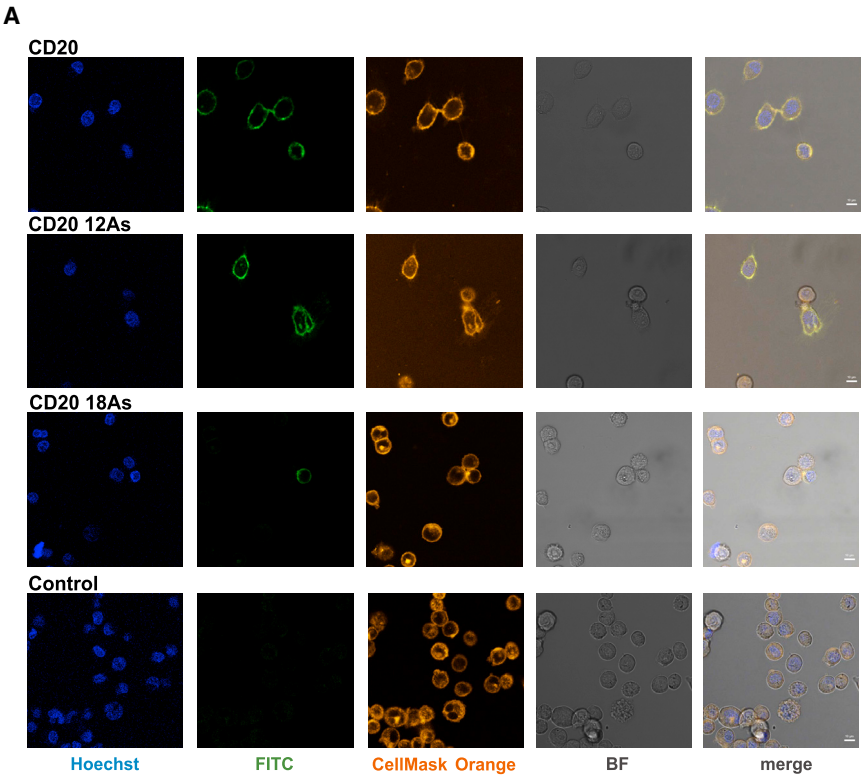

Figure 2. CD20 hypomorph live imaging and flow cytometry

(A) Fluorescence and bright-field (BF) microscopy images of live CHO cells expressing the CD20, CD20 12As, and CD18As constructs. CD20-positive cells were labeled using an anti-CD20-2H7 FITC-labeled antibody. The cell membrane is labeled with CellMask Orange stain. Control non-transfected CHO cells are indicated. DNA was labeled with Hoechst 33342 stain. The scale bar represents 10 μm. (B) Representative graphs showing flow cytometry scatterplots of CHO cells expressing CD20 and CD20 12As co-transfected with the mCherry construct. CHO cells expressing only mCherry and non-transfected cells are used as controls. The cells were stained an with anti-CD20-2H7 FITC-labeled antibody.

CRISPR-Cas9 insertion of poly(A) tracks in the TP53 endogenous locus in the near-haploid HAP1 cell line

With CRISPR-Cas9 technology development, a range of gene modifications, including point mutations, insertions, and deletions, can be made at precise genomic locations.[39] We wanted to find out whether endogenous hypomorphic mutants could be created using CRISPR-Cas9 technology to insert poly(A) tracks of various lengths into endogenous gene loci in human tissue cultures. Using this method, we created endogenous hypomorphic mutants in the *TP53* (tumor protein 53) gene and *AUF1* in HAP1 and HEK293 cells, respectively (Figures 4 and 5).

Guide RNAs (gRNAs) were designed to facilitate Cas9 nuclease activity in the fourth exon of the *TP53* gene (Figure S2). This gene locus encodes the loop region in the TP53 protein. We selected this position to assure targeting of the two major N-terminal isoforms of TP53 transcripts: canonical TP53, which contains the full N-terminal sequence, and Δ40TP53, which excludes the first 40 amino acids of the canonical TP53 isoform because of the presence of an internal start (AUG) codon (Figure 4A; Figure S2).[40] gRNAs were chosen for high NHEJ (non-homologous end joining) efficiency, low off-target effects, and proximity to the cut site. ssODN (single-strand oligo donor) DNA containing homology arms flanking the 3′ and 5′ regions of the poly(A) track insertion sequence (12As or 36As) was used as a template for CRISPR-mediated HDR (homology-directed repair) in the human near-haploid cell line HAP1.[41]

After CRISPR-Cas9 engineering of the *TP53* locus, we selected and confirmed by NGS (next-generation sequencing) and Sanger sequencing multiple cell clones containing an insertion of 12As or 36As (Figure S2). Engineered cell lines with successful insertion of poly(A) tracks in the single copy of the *TP53* gene in HAP1 cells were analyzed for mRNA stability and protein expression of the *TP53* gene using qPCR and western

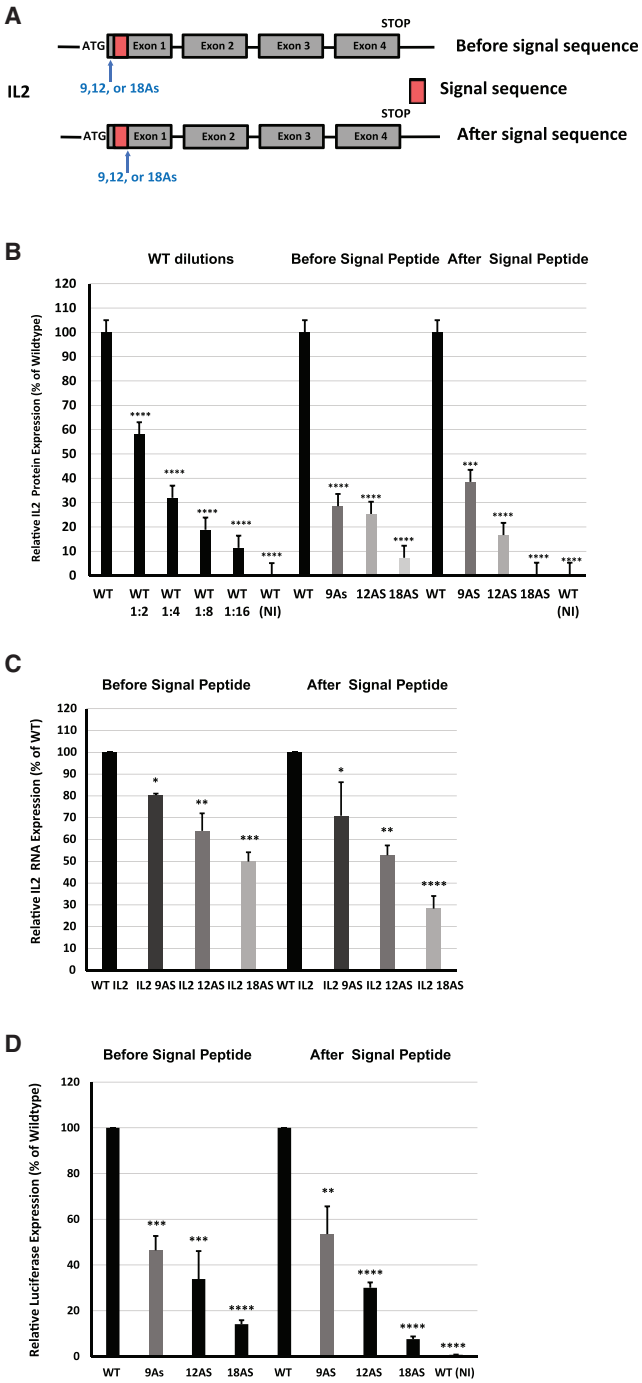

Figure 3. Effects of poly(A) insertions on IL-2 reporter expression, stability, and activity

(A) Scheme representative of poly(A) insertions and location of insertions for IL-2 reporter genes used in this study. Poly(A) insertions were placed before and after the signaling sequence (SS). IL-2 constructs containing the full-length WT IL-2 sequence and insertions of 9As, 12As, and 18As, respectively, were transiently expressed in HEK293 cells. Also shown is a schematic of the IL-2 gene with the start codon (ATG), termination codon (STOP), SS, exons, and insertion sites. (B) ELISA measured levels of IL-2 protein expression. IL-2 protein levels are calculated from cell supernatant collected from control (WT NI) HEK293 cells and cells expressing WT IL-2 and IL-2 with poly(A) tracks (9As, 12As, and 18As). A standard curve was used to obtain mean net absorbance. Dilutions of the supernatants from WT IL-2 (1:2–1:16) indicate linearity of the assay. (C) mRNA levels of IL-2 constructs were measured by qRT-PCR. IL-2 expression was normalized to β-actin. Relative mRNA and protein levels for control (–), WT IL-2, and IL-2 poly(A) track constructs (9As, 12As, and 18As) are presented as percentages of WT IL-2. (D) Biological activity of IL-2 was measured by the IL-2 bioassay (Promega). Relative IL-2 activity is measured by luciferase expression and normalized to supernatant of the WT IL-2 construct. Control (WT NI) and IL-2 poly(A) track constructs (9As, 12As, and 18As) are presented as percentages of WT IL-2. Error bars represent mean ± SD (n = 3). p values represent significance (*p ≤ 0.05, **p ≤ 0.01, ***p ≤ 0.001, ****p ≤ 0.0001).

blot analysis. GAPDH protein and mRNA levels were used as normalization controls between parental and engineered cell lines. Similar to the CD20 and IL-2 reporters, endogenous TP53 hypomorphs containing 12As or 36As had decreased mRNA levels and protein abundance, depending on the length of the inserted poly(A) track (Figures 4B and 4C). The 12A insertion reduced mRNA and protein amounts by 50% compared with WT TP53 expression in the original HAP1 parental line. Insertion of 36As resulted in almost complete loss of the TP53 protein and a 90% reduction in mRNA levels compared with TP53 levels in the original non-engineered HAP1 cells.

poly(A) tracks engineered in AUF1 endogenous loci of diploid HEK293 cells result in programmable hypomorphs

To test whether a CRISPR-Cas9 approach can be used to create poly(A) track hypomorphs in a human-derived diploid cell line, we targeted the AUF1 gene loci in the HEK293 T-Rex cell line (Invitrogen). As with the *TP53* gene, we introduced poly(A) tracks of 12As or 18As in the open reading frame of AUF1 (Figure 5; Figure S3). This time we engineered poly(A) tracks in the first exon of the *AUF1* gene after the second amino acid to assure targeting of all potential isoforms of AUF1 protein (Figure 5A).[42] After isolation of cell clones and confirmation of the poly(A) track insertion (Figure S3), cell lysates were analyzed for AUF1 mRNA levels and protein expression (Figures 5B and 5C). Similar to TP53, the mRNA stability and protein expression of endogenously engineered AUF1 hypomorphs were decreased in a length-dependent manner. Insertion of the poly(A) track of 12As led to a 50% and 40% reduction in protein and mRNA levels of AUF1, respectively. Insertion of 18As further reduced protein levels to approximately 10% of the parental cell line levels, whereas mRNA levels were reduced by 60%.

Hypomorphs of AUF1 affect mRNA levels of downstream target mRNAs

To test whether created hypomorphs with poly(A) insertions endogenously could be used to study the function of the gene with regard to established downstream targets, we performed expression analysis on TP53 and AUF1 hypomorphs (Figures 5D and 6). We measured the steady-state levels of the MAT1A, APP, TOP2A, and USP1 mRNAs in the parental HEK293 T-Rex cell line and the lines with engineered AUF1 hypomorphs (Figure 5D). MAT1A mRNA was previously stabilized by knockdown of AUF1, whereas transient knockdown of

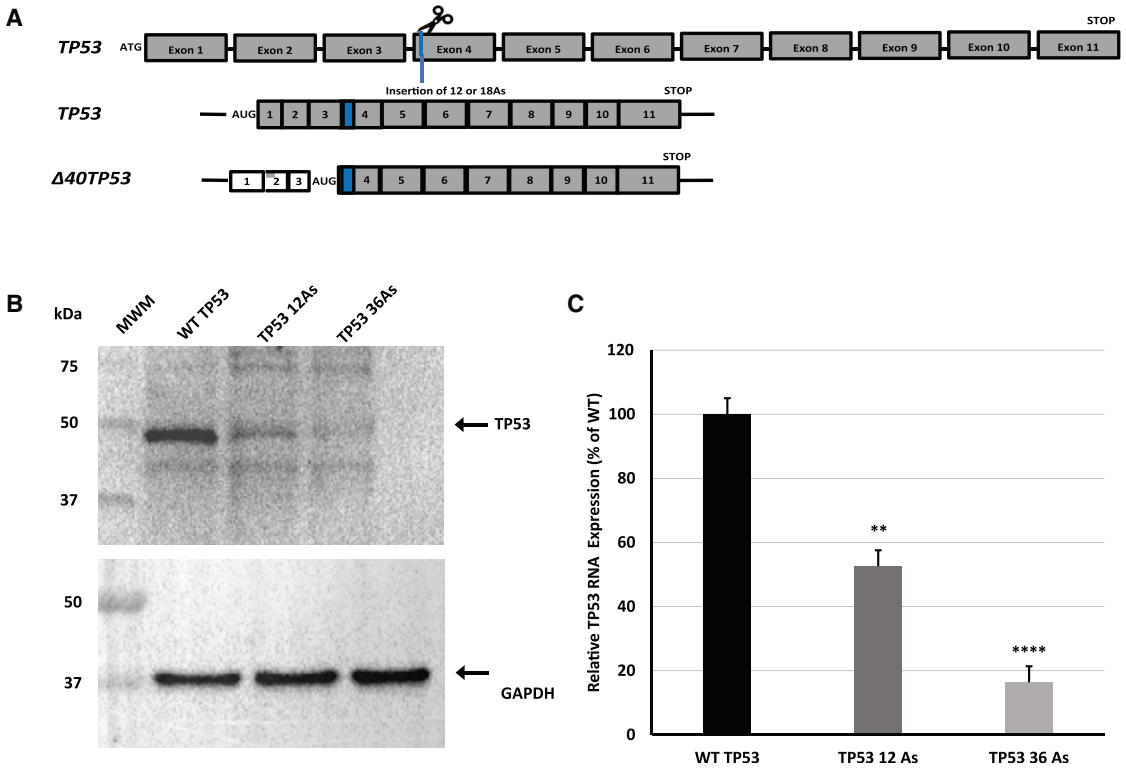

Figure 4. Creation and expression levels of endogenous TP53 poly(A) track hypomorphs in HAP1 cells using CRISPR-Cas9 genomic editing

(A) Cartoon representing the design of CRISPR-Cas9-mediated insertion of poly(A) tracks in the DNA sequence of TP53. The blue dashed line indicates the Cas9 (scissors) cleavage site and location of poly(A) track insertion (12As or 36As). The canonical and N-terminally truncated (delta 40) isoforms are shown with the engineered poly(A) tracks (blue). (B) Western blot analysis of WT HAP1 cells and HAP1 cells with endogenous poly(A) track insertions of 12As and 36As, respectively. Equal protein was used for analysis. TP53 was detected using a TP53-specific antibody. Constitutively expressed GAPDH was used as a loading control and was detected using a specific antibody. (C) The mRNA level of TP53 in WT HAP1 and TP53 hypomorphs was detected by qRT-PCR. TP53 expression was normalized to GAPDH mRNA expression. Relative mRNAs levels are presented as a percentage of WT TP53. Error bars represent mean ± SD (n = 3). p values represent significance (*$p \leq 0.05$, **$p \leq 0.01$, ***$p \leq 0.001$, ****$p \leq 0.0001$). Arrows indicate the positions of the full-length proteins.

AUF1 by small interfering RNA (siRNA) transfection induces destabilization of APP, TOP2A, and USP1 mRNAs.[34] Our results confirm the observations of previous studies.[24,25] MAT1A mRNA levels increase in the programmed hypomorphs of AUF1, whereas the levels of APP, TOP2A, and USP1 decline with a reduction in AUF1 expression. Even more compelling, the change in target gene mRNA levels was dependent on the length of the poly(A) track insertion and the extent of AUF1 reduction. Insertion of 18As has a more pronounced effect on mRNA stability than 12As (Figure 5D).

Hypomorphs of TP53 affect downstream genes in a dose-dependent manner

To extend our studies to potential use of programmable hypomorphs for gene dosage effects, we analyzed how insertion of poly(A) tracks in the *TP53* gene and reduction of *TP53* gene products affects downstream pathways known to be controlled or connected to TP53 protein. Based on previous studies and availability of antibodies, we selected BRCA1, DDIT4, DUSP6, MGMT, and P21 as TP53-associated genes.[43-49] We analyzed cell lysates by qPCR and western blot analysis (Figures 6A and 6B). We used parental HAP1 cells and engineered HAP1 cells with 12A and 36A insertions in the TP53 coding sequence (Figure 3). Tp53 protein and mRNA levels in these cells reflected WT TP53 levels, a 50% reduction in TP53 (TP53 12As), and nearly complete loss of TP53 protein (TP53 36As) (Figures 4B and 4C, 6A, and 6B). Western blot analyses indicated that BRCA1 levels did not change regardless of TP53 protein levels (Figure 6A). The protein levels of DUSP6 and DDIT4 showed differential behavior in the presence of the varying TP53 levels (Figure 6A). A 50% reduction of TP53 protein levels caused by insertion of a poly(A) track with 12As led to a significant reduction of DDIT4 and almost complete loss of DUSP6 protein in those cells (HAP1 TP53 12As). DDIT4 and DUSP6 were not affected or slightly increased in cells with almost complete loss of TP53 (HAP1 TP53 36As) compared with WT HAP1 cells. Finally, MGMT and P21 protein levels were severely depleted in cells expressing TP53 hypomorphs compared with WT HAP1 cells. Analyses of steady-state mRNA levels for all genes indicated the same trend as protein levels (Figure 6B). BRCA1 mRNA levels were unaffected in cell lines with different TP53 levels. DDIT4 and DUSP6 mRNAs showed a significant drop in levels, with a 50% TP53 protein reduction and WT or higher levels of

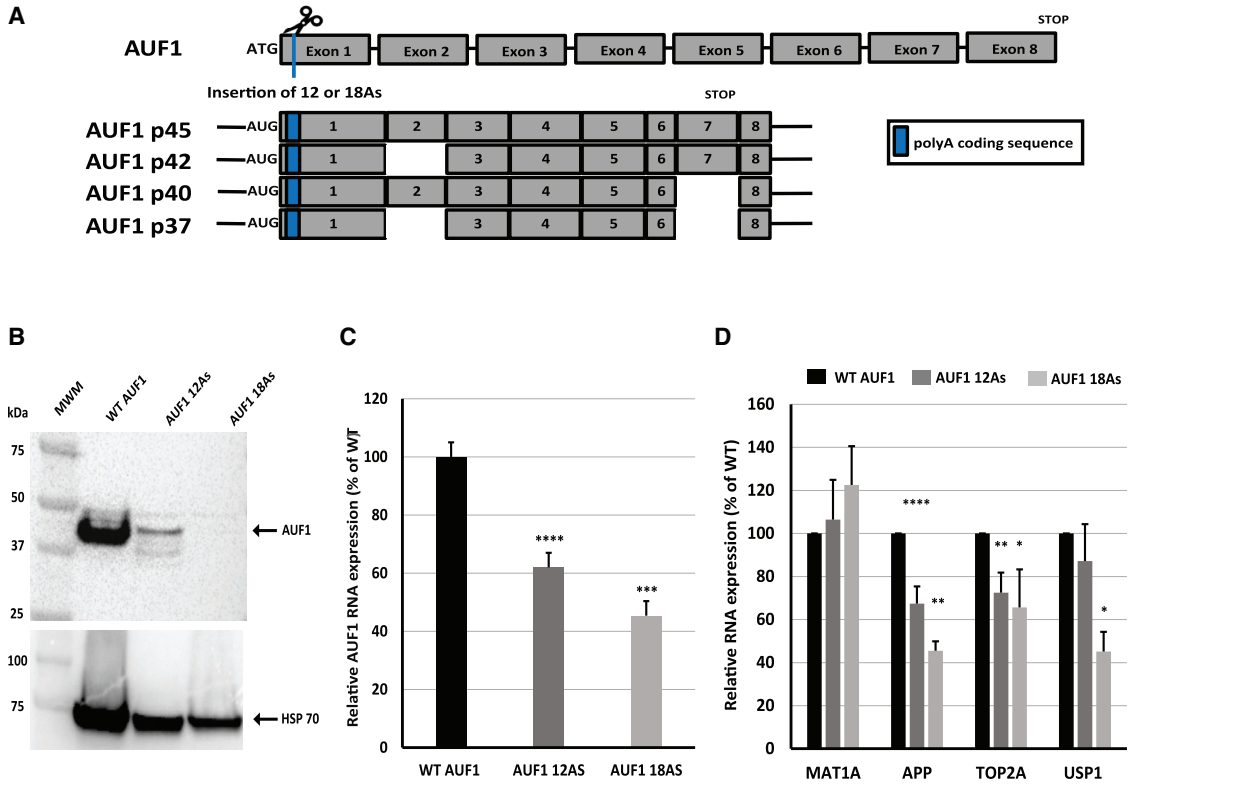

Figure 5. Design and gene-regulatory effect of endogenous AUF1 poly(A) track hypomorphs created using CRISPR-Cas9 genome engineering in HEK293 cells

(A) Cartoon representing the location of poly(A) track insertion in the DNA coding region of AUF1. The dashed blue line represents the Cas9 (scissors) cut site and location of poly(A) insertion (12As or 18As). Four of the major AUF1 mRNA isoforms (p45, p42, p40, and p37) are shown with their respective poly(A) insertions. (B) Western blot analysis of WT HEK293 cells and HEK293 cells with endogenous poly(A) insertions of 12As and 18As, respectively. Equal protein was used for analysis. AUF1 was detected with a specific antibody. Constitutively expressed HSP70 was used as a loading control and was detected using a specific antibody. (C) The mRNA level of AUF1 in WT HEK293 cells and AUF1 hypomorphs was detected by qRT-PCR. GAPDH was used for normalization of total mRNA levels. Relative mRNA levels are presented as a percentage of WT AUF1 as expressed in WT HEK293 cells. (D) The mRNA levels of the AUF1 downstream targets MAT1A, APP, TOP2A, and USP1 were detected by qRT-PCR. GAPDH was used to normalize total mRNA levels. Error bars represent mean ± SD (n = 3). p values represent significance (*$p \leq 0.05$, **$p \leq 0.01$, ***$p \leq 0.001$, ****$p \leq 0.0001$). Arrows indicate the positions of the full-length proteins.

mRNAs in cells with almost complete loss of TP53. Finally, MGMT and P21 mRNA levels were severely depleted in both TP53 engineered cell lines. We further tested whether TP53 and P21 levels can be changed when we apply hydroxyurea to HAP1 cells as a cytotoxic and genotoxic drug (Figure 6C).[50] We observed moderate increase in WT TP53 levels after 3- and 24-h treatment. Levels of TP53 with a 12A poly(A) track only changed after 24 h, and we did not observe detectable levels of TP53 with 36A insertion even after 24 h of hydroxyurea treatment. The P21 levels in the WT sample were induced after 3 h of hydroxyurea treatment and reduced after 24 h. Cells with 12A TP53 hypomorphic variants showed delayed induction of P21 levels only after 24-h hydroxyurea treatment, whereas cells with the 36A TP53 variant failed to show any induction of P21 even 24 h after hydroxyurea treatment (Figure 6C).

Finally, to test whether the poly(A) track hypomorphs can reproduce some of the results of gene mutations or deletions found in established cells from individuals with cancer, we obtained four TP53 mutant or deletion cell lines (Figure 6D) and focused on MGMT protein levels. Based on our hypomorphic models, we predicted that cell lines that contain less TP53 would contain less MGMT. In cell lines with WT TP53 status (HEK293 and MIA PaCa-2), MGMT protein expression was easily detectible. The SW620 cell line has a double mutation in the *TP53* gene (R273H/P309S) and deletion of the MGMT gene. As expected, TP53 protein levels were greatly reduced in the SW620 cell line, and MGMT protein expression was not observed. In the two cell lines that have negligible amounts of TP53 protein, PA14C (del - deletion of TP53) and K562 (Q136fs), MGMT protein levels were completely depleted (Figure 6D). These data indicate that our hypomorphic TP53 model can predict levels of the downstream gene MGMT.

DISCUSSION

In this study, we present a comprehensive method of creating hypomorphic mutations through insertion of poly(A) tracks. Using these

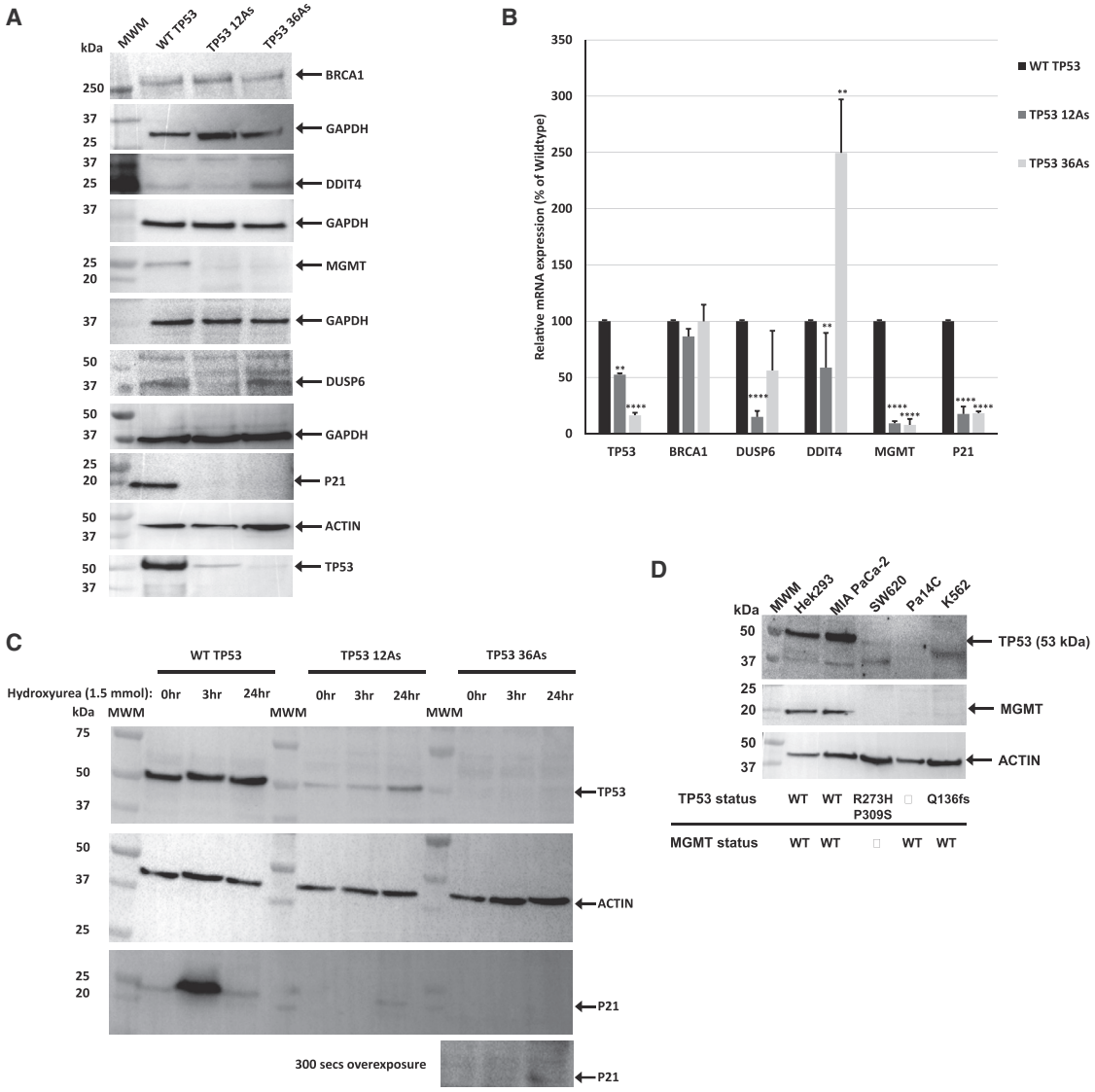

Figure 6. Effects of hypomorphic TP53 expression on the gene dosage of downstream targets

(A) Western blot analysis of BRCA1, DDIT4, DUSP6, MGMT, P21, and TP53 protein levels in WT and TP53 poly(A) track (12As and 36As) HAP1 engineered cells. Equal amounts of total protein were used for analysis. BRCA1, DDIT4, DUSP6, MGMT, P21, and TP53 expression was identified using a specific antibody. GAPDH and ACTIN were used as loading controls in each blot and were detected using specific antibodies. (B) BRCA1, DDIT4, DUSP6, MGMT, P21, and TP53 mRNA levels in WT and TP53 poly(A) track (12As and 36As) engineered cells. Relative mRNAs levels are presented as a percentage of the mRNA levels of the WT gene as expressed in WT HAP1 cells. (C) Western blot analyses of TP53 and P21 proteins in hydroxyurea-treated and control (NT - non treated) cells. The length of hydroxyurea treatment is indicated for WT and TP53 poly(A) track (12As and 36As) engineered cells. (D) Western blot analysis of TP53 and MGMT expression in HEK293, MIA PaCa2, SW620, Pa14C, and K562 cells. ACTIN was used to normalize total protein levels. Error bars represent mean ± SD (n = 3). TP53 and MGMT status are shown below (WT, wild-type; Δ, null). p values represent significance (*p ≤ 0.05, **p ≤ 0.01, ***p ≤ 0.001, ****p ≤ 0.0001). Arrows indicate the positions of the full-length proteins.

powerful gene-regulatory sequences, we show a method of creating hypomorphic mutations that is titratable and predictable (Figures 1, 2, 3, and 4). We expanded use of poly(A) track insertions to create hypomorphic mutants in integral membrane proteins (Figure 1). Integral membrane proteins make up 20%–30% of the proteome with highly diverse functions. Integral membrane proteins constitute the lipid bilayer of the membrane surrounding cellular organelles and the outside of the cell. They modulate movements of molecules and information across membranes and serve essential functions as signal receptors and transporters of solutes.[51,52] Their importance for cell function is apparent when these systems go awry; a substantial amount of disease-linked mutations occur in integral membrane proteins. Therefore, these proteins make up over 50% of US Food and Drug Administration (FDA)-approved drug targets.[53]

As a result of their significance in health and disease, we chose to demonstrate the ability to create hypomorphic mutations in the transmembrane B cell antigen CD20 (Figure 1). By inserting 12A or 18A nucleotides directly following the second amino acid, we observed that CD20 mRNA expression was reduced by 50% and 60%, respectively. Protein expression was similarly reduced for both poly(A) track-containing reporters. In addition to successfully reducing CD20 expression using this method, western blot analysis using a CD20 protein-specific antibody indicated expression of the full-length CD20 at the expected size of 33 kDa and the previously observed degradation product at 25 kDa.[29] Furthermore, our live-cell imaging and flow cytometry (Figure 2; Figure S1) indicated correct membrane localization and programmable reduction of membrane-inserted CD20 protein, supporting our hypothesis that introducing additional adenosine nucleotides at the N terminus of CD20 would not further affect localization and quality of the protein.[54] This result shows that N-terminal addition of the poly(A) track in other membrane genes may successfully create hypomorphic mutants.

Like membrane proteins, secretory proteins make up a large percentage of the proteome (~11%) and serve diverse functions as hormones, cytokines, and members of the extracellular matrix.[36,55,56] Because of these diverse functions, secretory proteins are essential for immune responses and cell-to-cell communication. Furthermore, the recent development of CAR-T cell therapies (Chimeric antigen receptor) indicates a need for attenuation of specific cytokines.[57] By creating hypomorphic mutations in alleles, these genes' functions can be examined or modulated, adding to the knowledge and significance of these genes in health and disease. With insertion of poly(A) tracks in these secretory genes, we wanted to ensure that these additions or mutations would not affect protein secretion by affecting the signal peptide's proteolytic cleavage. We used the cytokine IL-2 as a candidate because of the presence of a signal peptide at its N terminus (Figure 3).

To test the effect of poly(A) track placement on IL-2 RNA stability and secretion, we created gene reporters containing the complete coding sequence of IL-2 with poly(A) tracks of 9A, 12A, or 18A nucleotides inserted before or after the signal peptide (Figure 3A). Placement of the poly(A) track in IL-2 did not affect IL-2 secretion, as shown by the measurable amount and functionality of IL-2 protein in the supernatant of transfected HEK293 cells (Figures 3B and 3D). The mRNA stability of *IL2* and its protein expression were decreased for all constructs irrespective of the location of the poly(A) track insertion. Furthermore, as shown in our previous studies, in which we created hypomorphic reporter genes in eukaryotic cells, the decrease in IL-2 gene expression is titratable, meaning gene knockdown depends on the length of the poly(A) track.[19] Although the magnitude of IL-2 knockdown is greater in constructs with poly(A) tracks inserted after the signal peptide, this difference was not significant ($p < 0.05$) and was not clearly observed in a functional IL-2 assay (Figures 3B–3D). However, one can imagine that this discrepancy in IL-2 expression may result from the stalling and frameshifting mechanism of the poly(A) track.[16] Although the translational regulatory nature of the poly(A) track allows a decrease in gene expression for all constructs, the location may have a differential effect based on factors pertaining to mRNA quality control mechanisms.[58]

By combining our method with clustered regularly interspaced short palindromic repeat (CRISPR)-Cas9-based methods, we can create hypomorphic mutants endogenously. We tested this method by creating endogenous AUF1 and TP53 hypomorphs in diploid HEK293 cells and near-haploid human HAP1 cells, respectively (Figures 3 and 4). Introduction of 12As in the coding sequence of TP53 led to a decrease of ~40% in mRNA stability and protein expression. Endogenous insertion of 36As in the gene locus of the *TP53* led to an approximate 90% reduction in mRNA stability, and TP53 protein expression was nearly undetectable by western blot (Figure 3). After inserting poly(A) tracks of 12As and 18As in the coding region of AUF1, we saw reductions in the level of gene expression of approximately 40% and 60%, respectively. Protein expression of the four major isoforms ($p37^{AUF1}$, p40 ^{AUF1}, $p42^{AUF1}$, and $p45^{AUF1}$) showed similar levels of decrease in protein in expression (Figure 4). These results are consistent with previously observed eukaryotic reporter gene poly(A) track insertions of 12As and 36As.[19] The ~40% knockdown in TP53 and AUF1 in haploid and diploid cells, respectively, with insertion of 12As in each gene supports the predictability and effectiveness of this tool for various genes and cell types. By creating TP53 hypomorphs in the HAP1 line, we examined the effects of poly(A) track insertion on TP53 expression by mutating a single allele. The ability to create monoallelic hypomorphs using CRISPR-Cas9 and poly(A) tracks provides a feasible and straightforward method for studying phenotypes when expression of one allele is decreased.[59] Moreover, TP53 hypomorphs can be used to create a haploid state in haploid cells, such as HAP1, in which diploidization can occur.[59,60] Our titratable method for hypomorph creation may be able to maintain the haploid state through a P53 reduction without promoting the G1 cell cycle arrest and apoptosis that sometimes occur with deletion of P53.[61]

When creating titratable CRISPR-Cas9-engineered endogenous hypomorphs, we examined application of this tool for understanding the role of hypomorphic gene expression of *AUF1* and *TP53* in expression of their downstream targets. After observing the differential effects of addition of 12As or 18As on downregulation of AUF1, we assayed the effect of AUF1 protein reduction on previously defined targets, including *MAT1A*, *APP*, *TOP2A*, and *USP1*.[25,62] Because AUF1 has been demonstrated to stabilize or destabilize various targets, we expected that the reduction in AUF1 protein would have differential effects on expression of target mRNAs, depending on their previously established relationships.[63] For example, siRNA-mediated silencing of *AUF1* has been shown to stabilize expression of *MAT1A*.[24] Our results support this relationship between *AUF1* and *MAT1A*. Reduced expression of AUF1 in 12A and 18A hypomorphs lead to a moderate increase in *MAT1A* transcript expression slightly above WT levels (Figure 4D). Similarly, photoactivatable ribonucleoside-enhanced crosslinking and immunoprecipitation (PAR-CLIP) analysis identified post-transcriptional gene regulation of *APP*, *TOP2A*, and *USP1* by AUF1.[25] AUF1 was

found to interact with each mRNA through binding sites in the 3′ UTR and, together with the HuR protein, regulates translational efficiency and stability of target mRNAs. Our results show that the reduction in mRNA stability of each of these genes is related to the level of AUF1 downregulation, with a stepwise decrease in expression of these targets in 12A and 18A hypomorphs, respectively.

We determined the differential expression of TP53 against several cancer-related genes, including *BRCA1*, *DUSP6*, *DDIT4*, *MGMT*, and *P21* (Figure 6). Most notably, we observed that patterns of decreased TP53 expression do not necessarily correlate with the expression levels for downstream targets regulated by TP53. The differential effects of TP53 hypomorphs on DDIT4 and DUSP6 proteins is more than intriguing, given that these proteins are connected with TP53 status, the mammalian target of rapamycin (mTOR) pathway, cell metabolism, and proliferation.[45] There were also relatively stable levels of BRCA1 expression in both cells containing 12A or 36A insertions, whereas MGMT and P21 were decreased by more than 85% in both cell lines. Larger downregulation of MGMT and P21 than the level of TP53 expression has been supported by previous studies.[49,59,64] Our study allows a more quantitative and tunable approach to investigating the role of TP53 expression levels in modulation of downstream targets, accomplished previously with popular methods such as RNAi.[59] P21 levels under hydroxyurea treatment in TP53 poly(A) track-engineered cells showed a delay in induction compared with WT TP53 cells (Figure 6C).[50] In the case of MGMT, our tool's precision and predictability may have utility for uncovering a more cohesive role of TP53 downregulation on MGMT expression and how this regulation affects chemoresistance in certain cancers (Figure 6D).[49]

The utility of hypomorphic mutants created through poly(A) insertion can be seen in studies elucidating the function of proteins expressed in fungal pathogens such as *Candida albicans*. A recent study in *C. albicans* showed a decrease in protein abundance with insertion of poly(A) tracks of different lengths in the lanosterol demethylase (Erg11p) and penta-functional AROM polypeptide (Aro1p), common targets of antifungal agents.[20] The reduction of both genes' protein expression using this method was predictable, with insertion of six or more AAA codons causing a reduction in gene expression. Use of hypomorphic mutants created through poly(A) tracks in the prevalent pathogen, *C. albicans*, supports this tool's use in pathogenic microbes. With this tool, microbiologists can investigate the phenotypic effects of genetic manipulation in host organisms without use of xenobiotic agents and external environment changes. The results of this study and previous studies showing the effects of poly(A) track gene insertion undoubtedly support this tool's utility. The tool has been shown to be effective in eukaryotic and prokaryotic unicellular and multicellular organisms utilizing reporter constructs and CRISPR-Cas9. We predict that use of CRISPR-Cas9 for introduction of poly(A) tracks and generation of titratable and straightforward hypomorphic mutants will prove invaluable for synthetic biology and genetic studies.

MATERIALS AND METHODS

Cell culture

Hap1 TP53 cells were cultured in Iscove's Modified Dulbecco's Medium (IMDM) and supplemented with 10% Fetalgro and 5% penicillin and streptomycin (Gibco) and L-glutamine (Gibco). Flp-In T-REx 293 cells AUF1 cell line was cultured in Dulbecco's modified Eagle's medium (DMEM) (Gibco) and supplemented with 10% heat-inactivated fetal bovine serum (Gibco), 5% minimum essential medium nonessential amino acids (100×, Gibco), 5% penicillin and streptomycin (Gibco), and L-glutamine (Gibco).

Additionally, 5 μg mL^{-1} of blasticidin and 100 μg mL^{-1} of Zeocin were added to the medium for cell line maintenance. Flp-In T-REx 293 cells were cultured in Dulbecco's modified Eagle's medium (DMEM) (Gibco) and supplemented with 10% Fetalgro bovine growth serum (BGS), 5% minimum essential medium nonessential amino acids (100×, Gibco), 5% penicillin, streptomycin (Gibco), and L-glutamine (Gibco). Additionally, 5 μg mL^{-1} of blasticidin and 100 μg mL^{-1} of Zeocin were added to the medium for cell line maintenance. CHO-K cells were cultured in F-12K medium (Kaighn's modification of Ham's F-12 medium, Gibco) supplemented with 10% Fetalgro BGS, 5% minimum essential medium nonessential amino acids (100×, Gibco), 5% penicillin and streptomycin (Gibco), and L-glutamine (Gibco).

DNA constructs

IL-2 and CD20 constructs were created through PCR amplification from cDNA and genomic DNA, respectively. PCR products were purified using the Zymoclean Gel DNA Recovery Kit (Zymo Research) and cloned into the pEntryD-Topo vector. From the pEntryD-Topo vector, constructs were subcloned into the pcDNA-DEST40 or pcDNA-DEST53 vector for expression using LR clonase recombination (LR Clonase™ II kit, Thermo Fisher Scientific). Constructs were transformed using One Shot TOP10 chemically competent *E. coli* cells (Thermo Fisher Scientific). Sequences for plasmid DNA were confirmed by Sanger sequencing (Genewiz).

CRISPR/Cas9-mediated gene editing

CRISPR-Cas9 genomic editing was performed by the Genome Engineering and IPSC Center (GEIC) at Washington University. Single guide RNAs (sgRNAs) were designed according to sequences for TP53 and AUF1, respectively, acquired from the Ensembl genetic database. sgRNAs were selected based on off-target analysis performed by GEIC-specific algorithms. Ribonucleoproteins (RNPs) containing recombinant CRISPR-Cas9 and sgRNA were transfected to human cell lines using a Nucleofector (Lonza). Stable cell lines were generated by selection of hygromycin resistance. After assessment of Cas9 NHEJ nuclease activity by the Cel-1 assay, cell lines were propagated and assessed for positive insertion of poly(A) tracks by qRT-PCR and sequencing analysis (Figures S1 and S2). A more detailed description of these methods can be found in a publication from GEIC.[65]

Live imaging and flow cytometry of CD20-expressing cells

For live imaging, CHO-K cells were electroporated with a mCherry reporter, WT CD20, or CD20 constructs containing an insertion of 12As and 18As, respectively, with the Neon Transfection System (Thermo Fisher Scientific) using 100-μL tips and the cell line-specific protocol (https://www.thermofisher.com/us/en/home/life-science/cell-culture/transfection/neon-transfection-system/neon-transfection-system-cell-line-data.html). 24 h after electroporation, cells were washed twice with 1× PBS and blocked for 30 minutes with PBS/BSA buffer (PBS [pH 7.4] and 1% BSA). After blocking, cells were gently washed with 1× PBS before being incubated for 1 h in a 1:500 dilution of FITC-conjugated CD20 antibody (anti-human CD20 FITC 2H7, Thermo Fisher Scientific) in PBS/BSA buffer. Following incubation, cells were washed with 1× PBS prior to and after incubation for 1 h with a 1:8,000 dilution of Hoechst 33342 (Invitrogen) and 5 min with a 1:5,000 dilution of CellMask Orange plasma membrane stain (Invitrogen) in 1× PBS. Cells were washed twice with 1× PBS prior to imaging. Live fluorescence imaging was performed at the Washington University Center for Cellular Imaging (WUCCI). Cells were imaged using a Nikon A1Rsi scanning confocal microscope in wide-field mode and a Nikon CFI Plan Apochromat 20×/0.75 objective. Emission was filtered at 450 ± 50 nm (DAPI), 525 ± 25 nm (EGFP), and 595 ± 25 nm (mCherry/mTangerine). Cells were maintained at 37°C with 5% CO_2, controlled by a stagetop microscope incubation system (INU TIZW, TOKAI HIT, Japan).

For flow cytometry experiments, CHO-K cells were seeded at a density of 1.0×10^6 cells in a six-well plate 24 h before transfection. Cells were cotransfected with mCherry reporters and WT CD20 or CD20 constructs containing an insertion of 12As or 18As, respectively. 48 h after transfection, cells were trypsinized and pelleted. Cell pellets were washed twice with 1× PBS before being blocked with PBS/BSA buffer for 30 min on ice. After blocking, cell pellets were washed once with 1× PBS before 1-h incubation with a 1:500 dilution of FITC-conjugated CD20 antibody. Cell suspensions were filtered before FACS analysis using Partec North America CELLTRICS 100UM NS FLTR. Cytofluorimetric analysis was performed to enumerate CD20-positive and mCherry-positive CHO-K cells using the BD FACSCalibur system (BD Biosciences).

ELISA

Flp-In T-REx 293 cells were plated at a density of 1.5×10^6 cells in one well of six-well plates. Twenty-four hours after transfection with WT IL-2 or IL-2 constructs containing inserted poly(A) tracks, medium was collected. Medium was centrifuged at 1,500 rpm in a centrifuge at 4°C for 10 min, and cell supernatant was collected. The supernatant was used immediately or stored at −80°C. A solid-phase sandwich ELISA (Thermo Fisher Scientific, EH2IL2) was used to measure IL-2 concentration from cell supernatant according to the manufacturer's protocol (https://assets.thermofisher.com/TFS-Assets/LSG/manuals/MAN0014639_EH2IL2_ELISA_Kit_PI.pdf). Cell supernatant was diluted with complete cell medium at a ratio of 1:10 to be within the concentration of a range of the standard curve. Diluted cell supernatant was further diluted to obtain 1:2, 1:4, 1:8, and 1:16 dilutions using complete medium. Absorbance measurements were taken using the Synergy H4 hybrid multi-mode microplate reader (BioTek Instruments) at 450–550 nm. Concentrations were interpolated from standard curves created with GraphPad Prism statistical software.

IL-2 luciferase bioassay

According to the manufacturer's protocol, cell supernatant from untransfected cells and cells transfected with IL-2 constructs was diluted 1:12 with complete medium and used to perform the IL-2 bioassay (Promega, JA2201). Luminescence (RLU) was measured using the GloMax Explorer multimode microplate reader. Average RLU values were subtracted from background wells. Relative luciferase expression was measured in reference to samples from cells transfected with WT IL-2 constructs.

Hydroxyurea treatment

Hydroxyurea (Sigma-Aldrich) was kindly provided by Dr. Zhongsheng You. WT HAP1, HAP1 TP53 12A, and HAP1 TP53 18A cells were transferred into 12-well plates 24 h before hydroxyurea treatment. Hydroxyurea was added to the medium to a final concentration of 1.5 mmol. Non-treated and hydroxyurea-treated cells were collected 3 and 24 h after addition of hydroxyurea. Cell lysates were used for western blot analysis.

Western blot analysis

Total cell lysates for western blot analysis of TP53, AUF1, and CD20 hypomorphs were prepared with passive lysis buffer (Promega) and homogenized by passing five times through a 25G needle and syringe. Total protein was measured from cell lysis using the Bio-Rad DC Protein Assay according to the manufacturer's instructions (https://www.bio-rad.com/webroot/web/pdf/lsr/literature/LIT448.pdf). CD20 samples were prepared in 1× Bio-Rad XT sample buffer with 5% β-mercaptoethanol with equal total protein concentrations. Samples were boiled at 55°C for 10 min before loading on SDS-PAGE gel. AUF1 and TP53 samples were prepared in 1× Bio-Rad XT sample buffer with a 1× XT reducing agent. Samples were boiled at 95°C for 5 min before loading on SDS-PAGE gel.

The CD20 blot was blocked overnight in 5% milk (w/v) in 1× PBS with 0.1% Tween 20 (PBST). Blots were incubated in a 1:500 dilution of CD20 primary antibody overnight (Thermo Fisher Scientific, PA5-16701) and a 1:5,000 dilution of anti-GFP (Takara, 632381). Blots were washed (3 × 10 min) in TBST before and after incubation with a 1:10,000 anti-mouse secondary antibody (Cell Signaling Technology, 7076S) overnight. The blots were washed overnight before being incubated with a 1:5,000 dilution of anti-actin-horseradish peroxidase (HRP) for 2 h at room temperature (Cell Signal, 13E5).

The TP53, BRCA1, DUSP6, DDIT4, and MGMT blots were blocked overnight in 5% milk (w/v) in 1× PBST. All blots except for MGMT (incubated for 1.5 h at room temperature) were incubated overnight at 4°C in a 1:1,000 dilution with the following primary antibodies: anti-TP53 (Cell Signal, 2524), anti-BRCA1 (Abclonal, A11034),

anti-DUSP6 (Santa Cruz Biotechnology, 377070), anti-DDIT4 (Proteintech, 10638-1-AP), P21 (Cell Signal, 2947), and MGMT (Novus Biologicals, NB-100-168). Blots were washed (3 × 10 min) in TBST before and after incubation with a 1:10,000 anti-mouse secondary antibody (Cell Signal, 7076S) or 1:10,000 anti-rabbit secondary antibody (Cell Signal, 7074S) overnight. The blots were mildly stripped, washed vigorously, and blocked overnight in 5% milk (w/v) in 1× PBST before being incubated with a 1:5,000 dilution of anti--GAPDH-HRP (BioLegend, 649203) or a 1:2,000 dilution of anti-actin-HRP (5125).

The AUF1 blots were blocked overnight in 5% milk (w/v) in 1× PBST. The blots were incubated overnight at 4°C in a 1:2,000 dilution of anti-AUF1 antibody (Cell Signal, D6O4F). The blots were washed (3 × 10 min) in TBST before and after incubation with a 1:10,000 anti-rabbit secondary antibody (Cell Signal, 7074S). The blots were washed overnight before being incubated with a 1:5,000 dilution of anti-HSP70-HRP for 1 h at room temperature. All blots were washed 3 × 10 min in TBST before being developed with SuperSignal HRP substrate (Thermo Fisher Scientific). Images for all blots were generated by the Bio-Rad Molecular Imager ChemiDoc XRS System with Image Lab software.

RNA isolation and cDNA synthesis

Total RNA was extracted from Flp-In T-REx 293, CHO-K, and HAP1 cell pellets using the Illustra TriplePrep Kit (GE Healthcare Life Sciences) according to the manufacturer's instructions. An optional on-column DNase treatment was performed to remove genomic DNA (https://cdn.cytivalifesciences.com/dmm3bwsv3/AssetStream.aspx?mediaformatid=10061&destinationid=10016&assetid=13444). RNA concentration was measured by NanoDrop (optical density 260 [OD_{260}]/OD_{280}). One μg of total RNA was used to synthesize cDNA using SuperScript IV VILO Master Mix (Thermo Fisher Scientific).

qPCR analysis

qPCR was performed with iQ SYBR Green Supermix (Bio-Rad) in the Bio-Rad CFX96 real-time system using Bio-Rad CFX Manager 3.0 software. The IL-2 and CD20 constructs were identified using the forward primer 5′-CCCAAGCTGGCTAGTTAAGC-3′ and reverse primers 5′-GGTTTTGGACCAGATTGCAT-3′ and 5′-TCCAGCAGTAAATGCAGT-3′, respectively. All other genes in this study were identified using gene-specific primers.

Statistics

Statistical significances between control and experimental groups was calculated with unpaired Student's t tests using Graph Pad Prism v.9.1.2 (GraphPad, San Diego, California, USA). Analyses were performed separately for each experiment.

SUPPLEMENTAL INFORMATION

Supplemental information can be found online at https://doi.org/10.1016/j.omtn.2021.10.005.

ACKNOWLEDGMENTS

We thank Dr. Caitlin Hanlon and members of Djuranovic's lab for helpful comments. This work is supported by NIH R01 GM112824, NIH R01 GM136823, NIMH R01 MH116999, and Siteman Investment Program funds (to S.D. and S.P.-D.) and NIH T32 GM: 007067 and R25HG00668708 (to G.P.). We are also thankful to Ratner's Lab and the GEIC and WUCCI centers of Washington University for help with this project. The Washington University LEAP Gap Fund supported this project through the Skandalaris Center for Interdisciplinary Innovation and Entrepreneurship under award 1014, the Washington University Institute of Clinical and Translational Sciences, and NIH/National Center for Advancing Translational Sciences (NCATS) grant UL1TR002345. Poly(A) tracks technology is part of U.S. and international Patent Serial No. PCT/US2017/041766.

AUTHOR CONTRIBUTIONS

G.P. and S.P.-D. performed all experiments. G.P., S.P.-D., and S.D. performed data analyses and wrote the manuscript. S.P.-D. and S.D. conceived the project and provided funding. All authors were involved in editing the manuscript.

DECLARATION OF INTERESTS

The authors declare that they have no competing interests.

REFERENCES

1. Muller, H.J. (1932). Further studies on the nature and causes of gene mutations. Proc. 6th Int. Congr. Genet. 213–255.
2. Satokata, I., Ma, L., Ohshima, H., Bei, M., Woo, I., Nishizawa, K., Maeda, T., Takano, Y., Uchiyama, M., Heaney, S., et al. (2000). Msx2 deficiency in mice causes pleiotropic defects in bone growth and ectodermal organ formation. Nat. Genet. *24*, 391–395.
3. Ferretti, E., Villaescusa, J.C., Di Rosa, P., Fernandez-Diaz, L.C., Longobardi, E., Mazzieri, R., Miccio, A., Micali, N., Selleri, L., Ferrari, G., and Blasi, F. (2006). Hypomorphic mutation of the TALE gene Prep1 (pKnox1) causes a major reduction of Pbx and Meis proteins and a pleiotropic embryonic phenotype. Mol. Cell. Biol. *26*, 5650–5662.
4. St Johnston, D. (2002). The art and design of genetic screens: Drosophila melanogaster. Nat. Rev. Genet. *3*, 176–188.
5. Brenner, S. (1974). The genetics of Caenorhabditis elegans. Genetics *77*, 71–94.
6. Sin, O., Michels, H., and Nollen, E.A.A. (2014). Genetic screens in Caenorhabditis elegans models for neurodegenerative diseases. Biochim. Biophys. Acta *1842*, 1951–1959.
7. LaFave, M.C., and Sekelsky, J. (2011). Transcription initiation from within P elements generates hypomorphic mutations in Drosophila melanogaster. Genetics *188*, 749–752.
8. Boulin, T., and Bessereau, J.-L. (2007). Mos1-mediated insertional mutagenesis in Caenorhabditis elegans. Nat. Protoc. *2*, 1276–1287.
9. Boettcher, M., and McManus, M.T. (2015). Choosing the Right Tool for the Job: RNAi, TALEN, or CRISPR. Mol. Cell *58*, 575–585.
10. Heigwer, F., Port, F., and Boutros, M. (2018). RNA Interference (RNAi) Screening in *Drosophila*. Genetics *208*, 853–874.
11. Hemann, M.T., Fridman, J.S., Zilfou, J.T., Hernando, E., Paddison, P.J., Cordon-Cardo, C., Hannon, G.J., and Lowe, S.W. (2003). An epi-allelic series of p53 hypomorphs created by stable RNAi produces distinct tumor phenotypes in vivo. Nat. Genet. *33*, 396–400.
12. Doitsidou, M., Poole, R.J., Sarin, S., Bigelow, H., and Hobert, O. (2010). C. elegans mutant identification with a one-step whole-genome-sequencing and SNP mapping strategy. PLoS ONE *5*, e15435.

13. Schneeberger, K. (2014). Using next-generation sequencing to isolate mutant genes from forward genetic screens. Nat. Rev. Genet. *15*, 662–676.

14. Doitsidou, M., Jarriault, S., and Poole, R.J. (2016). Next-Generation Sequencing-Based Approaches for Mutation Mapping and Identification in Caenorhabditis elegans. Genetics *204*, 451–474.

15. Boutros, M., and Ahringer, J. (2008). The art and design of genetic screens: RNA interference. Nat. Rev. Genet. *9*, 554–566.

16. Arthur, L., Pavlovic-Djuranovic, S., Smith-Koutmou, K., Green, R., Szczesny, P., and Djuranovic, S. (2015). Translational control by lysine-encoding A-rich sequences. Sci. Adv. *1*, e1500154.

17. Koutmou, K.S., Schuller, A.P., Brunelle, J.L., Radhakrishnan, A., Djuranovic, S., and Green, R. (2015). Ribosomes slide on lysine-encoding homopolymeric A stretches. eLife *4*, 1–18.

18. Habich, M., Djuranovic, S., and Szczesny, P. (2016). PATACSDB—the database of poly(A) translational attenuators in coding sequences. PeerJ Comput. Sci. *2*, e45.

19. Arthur, L.L., Chung, J.J., Jankirama, P., Keefer, K.M., Kolotilin, I., Pavlovic-Djuranovic, S., Chalker, D.L., Grbic, V., Green, R., Menassa, R., et al. (2017). Rapid generation of hypomorphic mutations. Nat. Commun. *8*, 14112.

20. Tournu, H., Butts, A., and Palmer, G.E. (2019). Titrating Gene Function in the Human Fungal Pathogen *Candida albicans* through Poly-Adenosine Tract Insertion. MSphere *4*, e00192-19.

21. von Heijne, G. (1985). Signal sequences. The limits of variation. J. Mol. Biol. *184*, 99–105.

22. Johnson, A.E., and van Waes, M.A. (1999). The translocon: a dynamic gateway at the ER membrane. Annu. Rev. Cell Dev. Biol. *15*, 799–842.

23. Farhan, H., and Rabouille, C. (2011). Signalling to and from the secretory pathway. J. Cell Sci. *124*, 171–180.

24. Vázquez-Chantada, M., Fernández-Ramos, D., Embade, N., Martínez-Lopez, N., Varela-Rey, M., Woodhoo, A., Luka, Z., Wagner, C., Anglim, P.P., Finnell, R.H., et al. (2010). HuR/methyl-HuR and AUF1 regulate the MAT expressed during liver proliferation, differentiation, and carcinogenesis. Gastroenterology *138*, 1943–1953.

25. Yoon, J.-H., De, S., Srikantan, S., Abdelmohsen, K., Grammatikakis, I., Kim, J., Kim, K.M., Noh, J.H., White, E.J.F., Martindale, J.L., et al. (2014). PAR-CLIP analysis uncovers AUF1 impact on target RNA fate and genome integrity. Nat. Commun. *5*, 5248.

26. Stashenko, P., Nadler, L.M., Hardy, R., and Schlossman, S.F. (1980). Characterization of a human B lymphocyte-specific antigen. J. Immunol. *125*, 1678–1685.

27. Tedder, T.F., and Schlossman, S.F. (1988). Phosphorylation of the B1 (CD20) molecule by normal and malignant human B lymphocytes. J. Biol. Chem. *263*, 10009–10015.

28. Eon Kuek, L., Leffler, M., Mackay, G.A., and Hulett, M.D. (2016). The MS4A family: counting past 1, 2 and 3. Immunol. Cell Biol. *94*, 11–23.

29. Furusawa, Y., Kaneko, M.K., and Kato, Y. (2020). Establishment of C_{20}Mab-11, a novel anti-CD20 monoclonal antibody, for the detection of B cells. Oncol. Lett. *20*, 1961–1967.

30. Poly(A)k, M.J., and Deans, J.P. (2002). Alanine-170 and proline-172 are critical determinants for extracellular CD20 epitopes; heterogeneity in the fine specificity of CD20 monoclonal antibodies is defined by additional requirements imposed by both amino acid sequence and quaternary structure. Blood *99*, 3256–3262.

31. Li, R., Rezk, A., Miyazaki, Y., Hilgenberg, E., Touil, H., Shen, P., Moore, C.S., Michel, L., Althekair, F., Rajasekharan, S., et al.; Canadian B cells in MS Team (2015). Proinflammatory GM-CSF-producing B cells in multiple sclerosis and B cell depletion therapy. Sci. Transl. Med. *7*, 310ra166.

32. Vacher, P., Vacher, A.-M., Pineau, R., Latour, S., Soubeyran, I., Pangault, C., Tarte, K., Soubeyran, P., Ducret, T., and Bresson-Bepoldin, L. (2015). Localized Store-Operated Calcium Influx Represses CD95-Dependent Apoptotic Effects of Rituximab in Non-Hodgkin B Lymphomas. J. Immunol. *195*, 2207–2215.

33. Somasundaram, R., Zhang, G., Fukunaga-Kalabis, M., Perego, M., Krepler, C., Xu, X., Wagner, C., Hristova, D., Zhang, J., Tian, T., et al. (2017). Tumor-associated B-cells induce tumor heterogeneity and therapy resistance. Nat. Commun. *8*, 607.

34. Malek, T.R. (2003). The main function of IL-2 is to promote the development of T regulatory cells. J. Leukoc. Biol. *74*, 961–965.

35. Boyman, O., and Sprent, J. (2012). The role of interleukin-2 during homeostasis and activation of the immune system. Nat. Rev. Immunol. *12*, 180–190.

36. Zhang, L., Leng, Q., and Mixson, A.J. (2005). Alteration in the IL-2 signal peptide affects secretion of proteins in vitro and in vivo. J. Gene Med. *7*, 354–365.

37. Rogozhin, V.N., Logunov, D.Yu., Shchebliakov, D.V., Shmarov, M.M., Khodunova, E.E., Galtseva, I.V., Belousova, R.V., Naroditsky, B.S., and Gintsburg, A.L. (2011). An Efficient Method for the Delivery of the Interleukin-2 Gene to Human Hematopoietic Cells using the Fiber-Modified Recombinant Adenovirus. Acta Naturae *3*, 100–106.

38. Varshney, B., Agnihothram, S., Tan, Y.-J., Baric, R., and Lal, S.K. (2012). SARS coronavirus 3b accessory protein modulates transcriptional activity of RUNX1b. PLoS ONE *7*, e29542.

39. Doudna, J.A., and Charpentier, E. (2014). The new frontier of genome engineering with CRISPR-Cas9. Science *346*, 6213.

40. Hafsi, H., Santos-Silva, D., Courtois-Cox, S., and Hainaut, P. (2013). Effects of Δ40p53, an isoform of p53 lacking the N-terminus, on transactivation capacity of the tumor suppressor protein p53. BMC Cancer *13*, 134.

41. Carette, J.E., Raaben, M., Wong, A.C., Herbert, A.S., Obernosterer, G., Mulherkar, N., Kuehne, A.I., Kranzusch, P.J., Griffin, A.M., Ruthel, G., et al. (2011). Ebola virus entry requires the cholesterol transporter Niemann-Pick C1. Nature *477*, 340–343.

42. Raineri, I., Wegmueller, D., Gross, B., Certa, U., and Moroni, C. (2004). Roles of AUF1 isoforms, HuR and BRF1 in ARE-dependent mRNA turnover studied by RNA interference. Nucleic Acids Res. *32*, 1279–1288.

43. Arizti, P., Fang, L., Park, I., Yin, Y., Solomon, E., Ouchi, T., Aaronson, S.A., and Lee, S.W. (2000). Tumor suppressor p53 is required to modulate BRCA1 expression. Mol. Cell. Biol. *20*, 7450–7459.

44. Raimundo, L., Ramos, H., Loureiro, J.B., Calheiros, J., and Saraiva, L. (2020). BRCA1/P53: Two strengths in cancer chemoprevention. Biochim. Biophys. Acta BBA - Rev. Cancer *1873*, 188339.

45. Vadysirisack, D.D., Baenke, F., Ory, B., Lei, K., and Ellisen, L.W. (2011). Feedback control of p53 translation by REDD1 and mTORC1 limits the p53-dependent DNA damage response. Mol. Cell. Biol. *31*, 4356–4365.

46. Tirado-Hurtado, I., Fajardo, W., and Pinto, J.A. (2018). DNA Damage Inducible Transcript 4 Gene: The Switch of the Metabolism as Potential Target in Cancer. Front. Oncol. *8*, 106.

47. Piya, S., Kim, J.Y., Bae, J., Seol, D.-W., Moon, A.R., and Kim, T.-H. (2012). DUSP6 is a novel transcriptional target of p53 and regulates p53-mediated apoptosis by modulating expression levels of Bcl-2 family proteins. FEBS Lett. *586*, 4233–4240.

48. Grombacher, T., Eichhorn, U., and Kaina, B. (1998). p53 is involved in regulation of the DNA repair gene O6-methylguanine-DNA methyltransferase (MGMT) by DNA damaging agents. Oncogene *17*, 845–851.

49. Blough, M.D., Zlatescu, M.C., and Cairncross, J.G. (2007). O6-methylguanine-DNA methyltransferase regulation by p53 in astrocytic cells. Cancer Res. *67*, 580–584.

50. Ho, C.C., Siu, W.Y., Lau, A., Chan, W.M., Arooz, T., and Poon, R.Y.C. (2006). Stalled replication induces p53 accumulation through distinct mechanisms from DNA damage checkpoint pathways. Cancer Res. *66*, 2233–2241.

51. Shao, S., and Hegde, R.S. (2011). Membrane protein insertion at the endoplasmic reticulum. Annu. Rev. Cell Dev. Biol. *27*, 25–56.

52. Kar, U.K., Simonian, M., and Whitelegge, J.P. (2017). Integral membrane proteins: bottom-up, top-down and structural proteomics. Expert Rev. Proteomics *14*, 715–723.

53. Yildirim, M.A., Goh, K.-I., Cusick, M.E., Barabási, A.-L., and Vidal, M. (2007). Drug-target network. Nat. Biotechnol. *25*, 1119–1126.

54. Crockett, J.C., Mellis, D.J., Shennan, K.I., Duthie, A., Greenhorn, J., Wilkinson, D.I., Ralston, S.H., Helfrich, M.H., and Rogers, M.J. (2011). Signal peptide mutations in RANK prevent downstream activation of NF-κB. J. Bone Miner. Res. *26*, 1926–1938.

55. Benham, A.M. (2012). Protein secretion and the endoplasmic reticulum. Cold Spring Harb. Perspect. Biol. *4*, a012872.

56. Lorey, M.B., Rossi, K., Eklund, K.K., Nyman, T.A., and Matikainen, S. (2017). Global Characterization of Protein Secretion from Human Macrophages Following Non-canonical Caspase-4/5 Inflammasome Activation. Mol. Cell. Proteomics *16* (4, suppl 1), S187–S199.

57. Lee, Y.G., Chu, H., Lu, Y., Leamon, C.P., Srinivasarao, M., Putt, K.S., and Low, P.S. (2019). Regulation of CAR T cell-mediated cytokine release syndrome-like toxicity using low molecular weight adapters. Nat. Commun. *10*, 2681.

58. Arthur, L.L., and Djuranovic, S. (2018). Poly(A) tracks, polybasic peptides, poly-translational hurdles. Wiley Interdiscip. Rev. RNA *9*, e1486.

59. Olbrich, T., Mayor-Ruiz, C., Vega-Sendino, M., Gomez, C., Ortega, S., Ruiz, S., and Fernandez-Capetillo, O. (2017). A p53-dependent response limits the viability of mammalian haploid cells. Proc. Natl. Acad. Sci. USA *114*, 9367–9372.

60. Olbrich, T., Vega-Sendino, M., Murga, M., de Carcer, G., Malumbres, M., Ortega, S., Ruiz, S., and Fernandez-Capetillo, O. (2019). A Chemical Screen Identifies Compounds Capable of Selecting for Haploidy in Mammalian Cells. Cell Rep. *28*, 597–604.e4.

61. Stengel, A., Kern, W., Haferlach, T., Meggendorfer, M., Fasan, A., and Haferlach, C. (2017). The impact of TP53 mutations and TP53 deletions on survival varies between AML, ALL, MDS and CLL: an analysis of 3307 cases. Leukemia *31*, 705–711.

62. Frau, M., Tomasi, M.L., Simile, M.M., Demartis, M.I., Salis, F., Latte, G., Calvisi, D.F., Seddaiu, M.A., Daino, L., Feo, C.F., et al. (2012). Role of transcriptional and posttranscriptional regulation of methionine adenosyltransferases in liver cancer progression. Hepatology *56*, 165–175.

63. Gratacós, F.M., and Brewer, G. (2010). The role of AUF1 in regulated mRNA decay. Wiley Interdiscip. Rev. RNA *1*, 457–473.

64. Wang, X., Chen, J.X., Liu, J.P., You, C., Liu, Y.H., and Mao, Q. (2014). Gain of function of mutant TP53 in glioblastoma: prognosis and response to temozolomide. Ann. Surg. Oncol. *21*, 1337–1344.

65. Kouranova, E., Forbes, K., Zhao, G., Warren, J., Bartels, A., Wu, Y., and Cui, X. (2016). CRISPRs for Optimal Targeting: Delivery of CRISPR Components as DNA, RNA, and Protein into Cultured Cells and Single-Cell Embryos. Hum. Gene Ther. *27*, 464–475.